Ion-Pair Interaction in Pyridinium Carboxylate Solutions

Erik R. Berg,[‡] Daniel D. Green,[†] Diane C. Moliva A.,[†] Brady T. Bjerke,[†] M. W. Gealy,[‡] and Darin J. Ulness*[,†]

Departments of Chemistry and Physics, Concordia College, Moorhead, Minnesota 56562

Received: August 4, 2007; In Final Form: November 7, 2007

Ion-pair interactions between pyridinium cations and various carboxylate anions are explored using noisy light based coherent anti-Stokes Raman scattering ($I^{(2)}$CARS). Binary mixtures of pyridine and various carboxylic acids (including halo-acetic acids, straight-chain carboxylic acids, and pivalic acid) are prepared. A Brønsted type acid−base reaction occurs in these mixtures to create pyridinium and carboxylate ions. Both pyridine, itself, and pyridinium have strong $I^{(2)}$CARS signals originating from their ring breathing modes. The vibrational frequency of the ring breathing mode for pyridine is blue-shifted by hydrogen bonding, and that same mode for pyridinium is red-shifted by ion-pair interaction. Frequency shift data for the ring breathing mode of pyridine and pyridinium are presented. These data are discussed in terms of a simplistic model for the electronic behavior of these compounds.

I. Introduction

Organic-based ionic liquids (and solutions of organic salts) have received much attention in the literature because of their interesting properties.[1,2] Unlike simple liquids, ionic liquids have charge−charge based intermolecular forces. Cation−anion-pair interaction is therefore an important factor in determining the structure and dynamics of ionic liquids and, more generally, of solutions of organic salts.

This work focuses on solutions of pyridinium cations and various carboxylate anions. Pyridine is an important model molecule in biology as many drugs and metabolites are pyridine based. Further, the interaction of pyridine and its protonated form, pyridinium, with carboxylate groups is important in many ligand-binding pocket interactions.[3,4] Pyridine and pyridinium are also important compounds in synthetic chemistry both as ligands and, for the case of pyridine, as a solvent.[5] Here, we investigate binary mixtures of pyridine and a number of different carboxylic acids. The components of these mixtures react via a Brønsted type acid−base reaction in which the pyridine molecule becomes protonated by the carboxylic acid to form a pyridinium cation and a carboxylate anion. Because the acid−base reaction is product favored, high mole fraction values of the pyridinium cation and carboxylate anion can be achieved. By controlling the initial amounts of pyridine and carboxylic acid, one can explore a varity of final equilibrium conditions. Final conditions within the cuvette range from the case in which the pyridinium−carboxylate salt is solvated in excess pyridine to the case in which the salt is solvated in excess carboxylic acid.

The ring breathing mode (ν_1 mode[6,7]) of both the pyridinium cation and pyridine provides a useful spectroscopic signature for investigation of the interactions governing the structure and dynamics of these mixtures. Both hydrogen bonding to pyridine and protonation of pyridine into pyridinium perturb the ring breathing frequency enough to give rise to a separate distinct peak in the vibrational spectrum. Further, pyridinium in an ion-pair complex can be distinguished from freely solvated pyridinium via the frequency of the ring breathing mode. This work utilizes noisy light-based coherent anti-Stokes Raman scattering ($I^{(2)}$CARS)[8−21] to investigate the ring breathing mode of both the pyridinium cation and also pyridine itself. Both pyridinium and pyridine belong to the C_{2v} point group, and the ring breathing mode for each has A_1 symmetry and is strongly Raman active. A high quality $I^{(2)}$CARS signal can thus be obtained for this mode in both species.

A. Pyridine−Carboxylic Acid Systems. The carboxylic acids investigated in this work are collected in two groups. Group 1 consists of trifluoro acetic acid (TFAA), difluoroacetic acid (DFAA), trichloroacetic acid (TCAA), and group 2 consists of pivalic acid (2,2 dimethylpropionic acid), propionic acid, butyric acid, and octanoic acid. Acetic acid serves as the reference for both groups. The group 1 acids as compared with acetic acid vary strongly in pK_a (see Table 1) and are primarily modifying the electronic environment of the acid and the conjugate carboxylate base. The group 2 acids all have similar pK_a values but are primarily modifying steric bulkiness of the acid and the conjugate carboxylate base.

There is agreement in the literature that for mixtures of pyridine and carboxylic acids (and Brønsted systems in general), there are several different arrangements of ion−ion complexes (see Figure 1).[22−25] These include $pyH^+\cdots c^-$, $pyH^+\cdots c^-\cdots Hca$, and $pyH^+\cdots py$ among others. Freely solvated species are also present in addition to the above complexes.

Mixtures of pyridine and pyridine derivatives with various carboxylic acids have received attention in the literature over the past half-century.[21−28] Barrow, in 1956, used IR to study solutions of pyridine and carboxylic acids in chloroform.[22] In that work, a range of pK_a values was obtained using a number of different halo-acetic acids. That work was an important contribution to the understanding of ion-pair complexes in these systems. Since then, pyridine/carboxylic acids have been studied both in the liquid phase[21−28] and in the solid phase[29] and also by various techniques including NMR,[25] thermocalorimetry,[30] X-ray,[29] and several other methods. Indeed, recently, Limbach et al., offered a means of correlating NMR parameters with

[†] Department of Chemistry.
[‡] Department of Physics.

10.1021/jp076260l CCC: $40.75
Published on Web 01/12/2008

TABLE 1: Standard (25 °C) pK_a Values for the Carboxylic Acid Studied in This Work.

carboxylic acid	pK_a	carboxylic acid	pK_a
acetic acid	4.75	propionic acid	4.87
trifluoroacetic acid	0.23	*n*-butyric acid	4.82
difluoroacetic acid	1.34	*n*-octanoic acid	4.89
trichloroacetic acid	0.70	pivalic acid	5.03

hydrogen-bonded and ion-pair structures in these systems, which provides new insight into characterizing the proton exchange energy profile between acid−base pairs.[25] Also, small clusters of pyridine/carboxylic acid system were produced via vacuum adiabatic expansion and analyzed via mass spectrometry.[24] That work provided much insight into these systems in polar solvents including water. Thus, pyridine/carboxylic acid systems are still an important subject of study.

Some Raman work on the pyridine/acetic acid system has been done. Mierzecki[26] in 1960, Singurel and Bazhulin[27] in 1967, and Rezaev and Tabibi[28] in 1976 each present an extensive dilution study for this system. Very recently, Berg et al.[21] presented I$^{(2)}$CARS results for both dilution and temperature studies of this mixture. All these works report a dominant peak that is blue-shifted ∼14−16 cm^{-1} from the ring breathing peak of free pyridine. These works also report a weak peak developing at low X_{py} values. Mierzacki attributes this weak peak to water contamination.[26] Studies by Singurel and Bazhulin, and Berg et al., both suggest that the dominant peak is from a pyridinium cation−acetate anion-pair complex (Figure 1a) and the weak peak is from the free pyridinium ion.[21,27] The current work supports the latter view as well. The authors were unable to locate Raman-based studies of pyridine with the other acids used in this work.

Another interesting feature of the I$^{(2)}$CARS signal from pyridinium is the strong suppression of the triangle mode. A rigorous explanation of this behavior cannot be given here; however, a heuristic argument can be made. The pyridinium cation is very similar in structure to benzene. Benzene has D_{6h} symmetry, so its triangle mode (B_{1u}) is not Raman active by symmetry. The pyridinium cation is still a member of the C_{2v} point group, so one cannot rigorously use symmetry to explain the strong suppression of the triangle mode. Nonetheless, the benzene-like nature of the pyridinium cation might underlie the observed results. Indeed, benzene has been used as a model for pyridinium in lieu of experimental data for pyridinium itself.[31]

B. Simple Model for the Electronic Behavior of Pyridine and Pyridinium. A simple model of the electronic behavior of pyridine upon hydrogen bonding and protonation by an acid was presented in ref 21, which used a qualitative molecular orbital picture and simple electrostatic arguments. For convenience the description of the model is repeated below. This model is clearly a gross oversimplification of changes in electron distribution in pyridine, nonetheless it provides a simple picture that seems to be consistent with all of the results of this work. Moreover, this model provides a basis for the understanding of the results for the different carboxylic acids used in this study as well as that of Berg et al.[21]

Without protonation (or a hydrogen bond), free pyridine has a lone pair of electrons in an sp^2 hybrid orbital localized on the nitrogen atom. Due to the relatively large spatial extent of the orbitals of the nonbonded lone-pair electrons, the delocalized π molecular orbital gets squeezed out of the region and this destabilizes the π contribution to the ring bonds relative to a hypothetical situation where there is no lone pair of electrons on the nitrogen. When protonation or hydrogen bonding occurs, some of the lone-pair electron density gets drawn out by the hydrogen, thereby releasing the "squeeze" on the π orbital. This allows more delocalization of the π electron density and stabilizes the system, resulting in a blue shift of the ring breathing mode. Figure 15 of ref 21 expresses the essential aspects of the model in pictorial form.

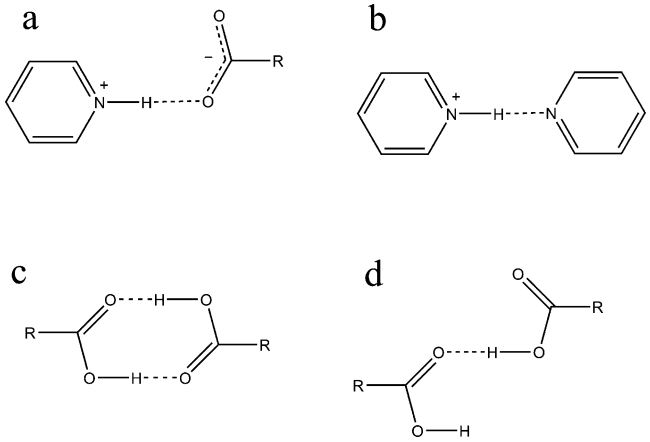

Figure 1. Some representative examples of the many ion−ion and hydrogen bond pairings in pyridine/carboxylic acid mixtures. (a) Ion-pair complex between the pyridinium cation and a carboxylate anion. (b) Pyridinium−pyridine hydrogen-bonded complex. (c) Cyclic-pair carboxylic acid dimer. (d) Open-extended-chain carboxylic acid network.

The reader is directed to a recent substantial study by Krygowski et al., of 397 pyridine and pyridinium compounds in the Cambridge Structural Database.[5] That work characterized aromaticity in a standard way via HOMA (harmonic oscillator model of aromaticity) values. It was found that hydrogen bonding to pyridine (and from pyridinium) causes little change in ring geometry and π density. The above effect captured by the simple electrostatic/molecular orbital is subtle but evidently significant enough to cause a small but clearly noticeable shift in the ring breathing frequency of pyridine by about 0.5−1%.

The results reported in ref 21 show that the blue shift of the ring breathing mode increases from formamide to water to acetic acid. A stronger hydrogen bond will draw out more of the lone-pair electron density. Complete protonation will draw out the most lone-pair electron denisty. This relieves the squeezing of the π molecular orbital to a greater degree causing more stabilization and a greater blue shift of the ring breathing mode. This picture is also consistent with the assignment of a "redder" ring breathing peak of the pyridinium cation to an ion-pair complex and a "bluer" ring breathing peak to free pyridinium. The presence of the counteranion near the hydrogen attached to the nitrogen in the pyridinium cation draws back the partial positively charged hydrogen to some degree. This weakens the coordination to the nitrogen relative to the case when no anion is present. On the basis of the current qualitative argument, the ion-pair complex should then have a ring breathing mode that is to the red of the free pyridinium cation. Further, stronger ion-pair interaction will increase the red shift of the ring breathing mode relative to the freely solvated pyridinium (and decrease the blue shift relative to that for pyridine).

Incidentally, this model is also consistent with the strong suppression of the triangle mode of pyridine. The argument used above was that, in spite of C_{2v} symmetry, the "benzene-like" nature of pyridinium resulted in suppression of the triangle mode. The simple molecular orbital/electrostatic picture also suggests an electronic environment that becomes more benzene-like upon protonation of pyridine. The I$^{(2)}$CARS signal, like

any CARS signal, originates from the polarizability of the electron density.

II. Overview of I$^{(2)}$CARS

The I$^{(2)}$CARS experiment, its theoretical description, and the data analysis methods have been well described in the literature.[8−21] Here we provide only an overview of each of these aspects of I$^{(2)}$CARS and direct the reader to the literature for a more thorough treatment.

A. I$^{(2)}$CARS Experiment. The I$^{(2)}$CARS experiments were performed in the standard way.[8,10,15−17] The noisy light source was made by removing the frequency selective grating from a pumped dye laser (Spectra Physics) containing rhodamine 640 (Exciton). This allows the entire lasing spectrum (peak at 600 nm) of the dye to be emitted in a phase incoherent way. A second pumped dye laser (Spectra Physics) containing DCM (Exciton), which was operating normally, was used as the narrowband source, M. Both dye lasers were pumped at 10 Hz by a Nd:YAG laser (Spectra Physics).

The noisy beam was split into twin beams, B and B′, by a Michelson interferometer. A stepper motor (Newport) was used to translate the retroreflecting mirror in one arm of the interferometer. This introduced a controllable time delay between B and B′. The stepper motor was calibrated using the well characterized I$^{(2)}$CARS signal from benzene. The twin noisy beams emerged from the interferometer running parallel to one another with a separation of approximately 2 mm on-center. They were joined with the narrowband beam in the standard BOX beam configuration. The three beams were focused onto the sample using a 150 mm focal length lens. The beam energies at the sample were on the order of tens of microJoules per pulse. The I$^{(2)}$CARS signal emerged along its own wavevector and was spatially isolated using an iris. The signal was then directed into a spectrometer (SPEX) and ultimately onto a 100 × 1340 pixel array, liquid nitrogen-cooled CCD detector (Roper Scientific/Princeton Instruments). This spectral dimension of the experiment was calibrated using neon lines. The absolute resolution of the spectrometer, as characterized by the half-width at half-maximum of the neon lines, was found to be 0.38 cm^{-1}. I$^{(2)}$CARS spectra were collected at each delay setting to produce the spectrogram. All spectrograms were produced by moving the stepper motor over a range from −1.00 to 1.00 mm in steps of 0.01 mm. At each delay a ten-shot average spectrum was recorded. Typically, five complete spectrograms were averaged for each sample (more when signals were weak). Each spectrogram took approximately 8 min to acquire.

All samples were used as received with no further purification. Mole fraction mixtures, of approximately 15 mL total volume, were created using either class A burets or graduated pipets. The error in mole fraction is estimated to be less than 0.7%. Temperature control of the samples was done using a home-built brass jacket and a recirculating bath (FTS Systems). The temperature was held constant to within ±0.2 °C. During the experiment the samples were contained in a 2 mm glass cuvette (Starna) with a Teflon stopper.

For several of the mole fraction compositions involving the halo-acetic acids, a solid pyridine-halo-carboxylate salt was formed at room temperature. In these cases, the samples were melted/made to dissolve in a sand bath, transferred to the sample cuvette, and data were collected at 65 °C. Nearly equal molar and equimolar mixtures of TFAA/pyridine and TCAA/pyridine formed salts that remained solid above 75 °C—the upper limit of the controllable temperature jacket.

B. Results from I$^{(2)}$CARS Theory. The analytic results for the I$^{(2)}$CARS signal intensity, $I(\omega_D,\tau)$, as a function of detected frequency (ω_D) and interferometric delay time (τ) are presented here. The material response function is taken to decay exponentially (Lorentzian line shape) and the noisy light is taken to have a very broad Lorentzian spectral density. An important property I$^{(2)}$CARS exhibits is that signals from individual Raman active modes within the sample simply add. There is no quantum beating between the signals from different modes. For the component of the signal from a given mode, the frequency and delay-time dependent I$^{(2)}$CARS signal intensity is approximately given by

$$I(\omega_D,\tau) \propto J(\omega_D)e^{-2\gamma|\tau|}\left(\frac{\cos(\Delta_{CARS}\tau)}{2\gamma}\right) + \frac{R}{2\gamma}e^{-2\gamma|\tau|}\sin(\Delta_{CARS}|\tau|) + I(\omega_D,\infty) \quad (1)$$

where $I(\omega_D,\infty)$ is the τ-independent background term. In this expression, $J(\omega_D)$ is the spectral density of the broadband light and R is the nonresonant to resonant ratio of the orientationally averaged third-order hyperpolarizabilities.[12] $\Delta_{CARS} \equiv 2\omega_R + \omega_M - \omega_D$, where ω_M is the frequency of the monochromatic beam and ω_D is the detected frequency. The frequency Δ_{CARS} vanishes at the zero difference frequency,[18−20] ω_D^0; here $\omega_R = (\omega_D^0 - \omega_M)/2$ gives the precise Raman vibrational frequency. The observed decay rate constant, $\gamma = \gamma_R + \gamma_I/2$, where the instrument response, γ_I, is due to a finite slit width of the monochromator and a finite bandwidth of the monochromatic beam. Γ is the (Lorentzian) bandwidth of the broadband fields.

C. Data Fitting. With a multipeak version of expression (1) as the guide from theory, the I$^{(2)}$CARS spectrograms for each of the pyridine mixtures were fit using MATHEMATICA which employs the Marquardt−Levenberg version of nonlinear least-squares regression.[32,33] For I$^{(2)}$CARS the Raman frequency of a given mode is determined by the zero difference frequency, $\omega_{D_i}^0$, provided ω_M is accurately known and the signal detection window is correctly calibrated. For frequency differences, ω_M need not be calibrated, so any uncertainty associated with ω_M does not appear in the frequency shift measurements—an advantage of the method.

D. x-Marginal Spectra. As mentioned earlier, data are collected in the form of a spectrogram. When Fourier-transformed from time-frequency dimensions to frequency−frequency dimensions, the spectrogram method of detection provides a valuable visual representation of the signal (see Figure 2). The visually apparent x pattern in the transformed spectrogram allows one to unambiguously see Raman modes that are not evident in the raw spectrogram nor would be strongly present in a spectrum representation. Nevertheless, it is difficult to compare one transformed spectrogram to another in anything other than a very gross qualitative way.

Therefore one additionally compresses the visual information carried by the two-dimensional picture of the Fourier-transformed spectrogram by computing what is called the x-marginal spectrum.[20,21] The utility of the x-marginal procedure is to imitate what the human eye does in recognizing the characteristic x pattern of a Raman mode. A narrow (0.6 cm^{-1}) x shaped mask is defined such that the slopes of the lines making up the x mask match the slopes of the x pattern of the Raman mode. The mask has a value of unity within the defined x shape and zero outside of it. The Fourier-transformed spectrogram is multiplied by the mask leaving nonzero values within the x area. The result is then summed up to give a single value called the x-marginal. The center of the mask is then moved to the adjacent pixel value and the procedure is repeated to give another

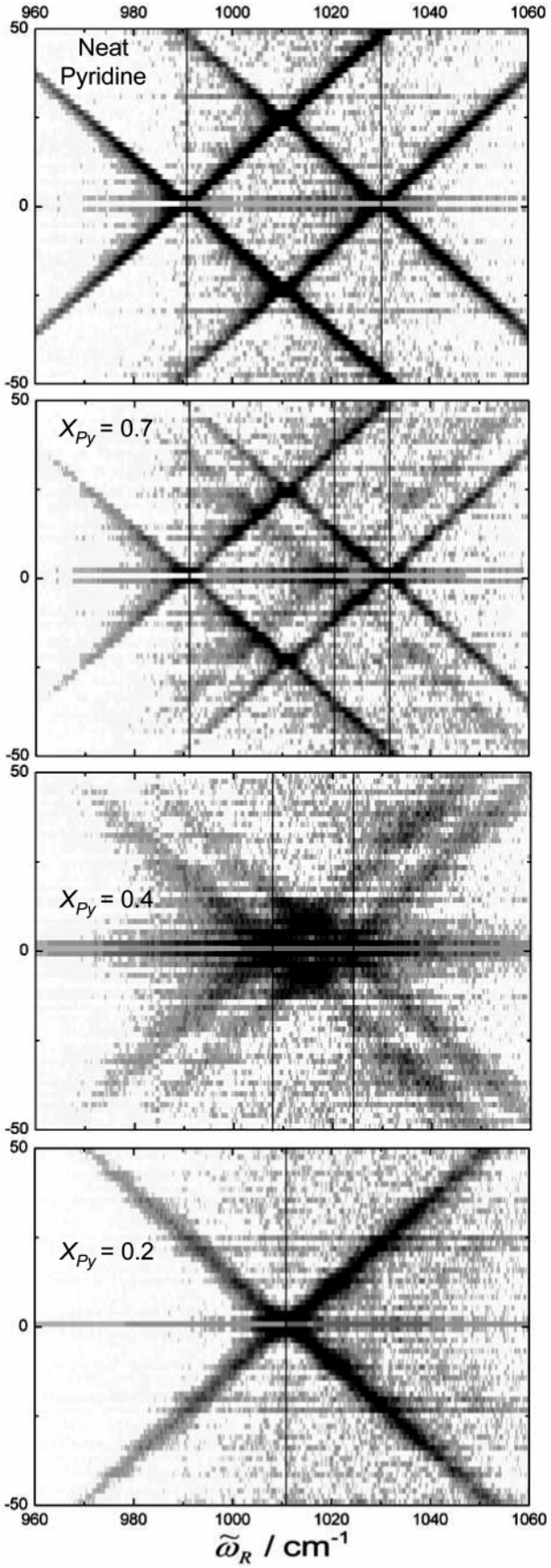

Figure 2. Fourier-transformed $I^{(2)}$CARS spectrograms for pyridine/TFAA mixtures. The different $I^{(2)}$CARS active vibrational modes appear as a characteristic x pattern in the spectrograms. The vertical lines are to guide the eye in noticing wavenumber shifts in these modes at the various mole fractions.

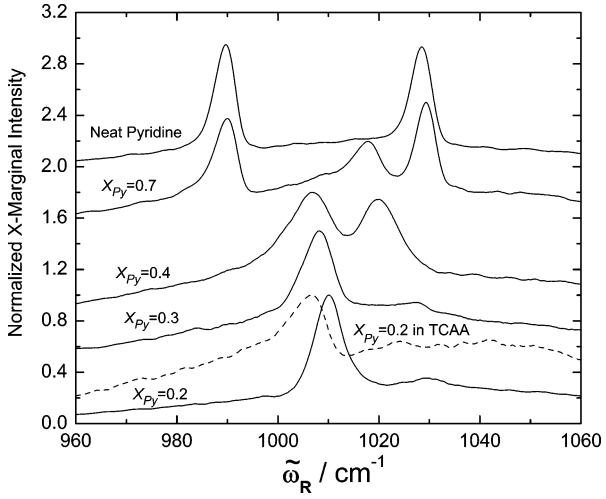

Figure 3. Normalized x-marginal spectra for pyridine/TFAA (solid line) and pyridine/TCAA (dashed line) mixtures. See text for a discussion of the qualitative features of these spectra.

x-marginal value. When the x mask is centered over an x shaped Raman mode the x-marginal is large, conversely when the x mask is not centered over the Raman mode the x-marginal is small (but not zero). As the center position of the x is scanned across the Fourier-transformed spectrogram a collection of x-marginals is produced to form an x-marginal spectrum.

It is important to keep in mind that the x-marginal spectra do not provide precise quantitative data regarding the parameters of the material model. Quantitative data are obtained from fitting the spectrograms themselves. The x-marginal spectra simply provide a concise qualitative representation of the data contained in the spectrograms.

III. Results and Discussion

The pyridine/TFAA system yields results that are quite different from the pyridine/acetic acid system reported in the literature.[21,26,27] In the pyridine/TFAA system at high mole fraction values of pyridine, the solvated pyridinium ion is favored over the pyridinium−TFA^- ion pair (Figure 1a). This is most clearly seen in the $X_{py} = 0.7$ curve in Figure 3. The peak at 1020 cm^{-1} is the ring breathing mode of unpaired pyridinium. The absence of a peak at approximately 1008 cm^{-1} indicates the pyridinium−TFA^- ion pair is not a major component of the mixture at this mole fraction (although presumably present to some degree at a level under the noticeable limits of $I^{(2)}$CARS). The peaks at 990 and 1030 cm^{-1} indicate the presence of free pyridine. The $X_{py} \leq 0.3$ curves in Figure 3 show a single peak at ~1008 cm^{-1}, indicating that the predominant pyridine-based species is the pyridinium cation which is ion-paired with a TFA^- anion. At this mole fraction, freely solvated pyridinium is not present at an amount sufficient to produce a detectable $I^{(2)}$CARS signal. The curve at $X_{py} = 0.4$ shows that ion pairs and unpaired pyridinium are both present in the sample.

It is interesting to note that there is no evidence of a significant amount of pyridine-pyridinium hydrogen-bonded complexes (Figure 1b). Such complexes would appear in Figure 3 as a peak at ~994 cm^{-1} because N−H−N hyrdrogen bonds are known to cause a blue shift of approximately 4 cm^{-1}.[21] A more subtle feature seen in Figure 3 is a blue shifting of the ring breathing mode of both the ion-paired and freely solvated pyridinium ion.

The simple electrostatic/molecular orbital model for pyridine and pyridinium, which was outlined in the Introduction section,

can be applied to understand the results of the pyridine/TFAA acid study. It is well-known in synthetic chemistry that TFA^- is relatively non-intrustive. In fact, TFA^- is often chosen as a counterion when one desires minimal ligand coordination. Indeed it is a less competitive ligand than pyridine.[34] The principle reason for this property of TFA^- is the high electronegativity (and hence the electron withdrawing ability) of the fluoride atoms. This also makes TFAA a much stronger acid than acetic acid ($pK_a = 0.26$ versus $pK_a = 4.76$) and consequently TFA^- a much weaker conjugate base than acetate. With this in mind, one can qualitatively understand the $I^{(2)}$CARS results for the pyridine/TFAA system. The first interesting aspect of this system is the emergence of the non-ion-paired pyridinium at high X_{py} values. The situation in the cuvette under these conditions is one in which there are three principle species: pyridine, pyridinium ion, and TFA^-. The electrostatic interaction between the pyridinium cation and the TFA^- anion is not sufficient to form a significant number of ion-pair complexes. This is consistent with the weak coordinating nature of TFA^-. The pyridine itself is more competitive than the TFA^- for interaction with pyridinium. There is, however, a curious "non-result". One might anticipate the formation of a pyridine−pyridinium hydrogen-bonded pair (Figure 1b). There is no evidence in the $I^{(2)}$CARS data that this hydrogen-bonded complex exists at a significant mole fraction. Presumably, there is significant interaction between pyridine and pyridinium,[35] but the proton transfer from pyridinium to pyridine is evidently sufficiently fast that, on the time scale of the $I^{(2)}$CARS signal generation (several picoseconds), there is not a significant number of truly hydrogen-bonded metastable complexes. We were unable to find independent support of this presumption in the literature. This understanding is not entirely satisfying especially in light of the clear evidence for long-lived (> several picoseconds) hydrogen-bonded complexes of pyridine with a variety of hydrogen bond donors.[21,36−39]

The blue shift of the ring breathing mode of the ion-paired pyridinium with dilution with TFAA can also be understood using the simple model. At low X_{py} values the pyridinium/TFA^- ion-pair complex is solvated predominantly by TFAA rather than with pyridine. There is a strong hydrogen bond interaction (and even potential proton transfer) between the TFAA and the TFA^- anion. This diverts some of the electron density away from the H^+-O^- interaction with pyridinium. Hence the ion pairing is slightly weakened and by the simple model, the ring breathing mode should shift to the blue (the pyridinium in the ion pair is behaving more like freely solvated pyridinium.)

The effect of acid strength, or more directly conjugate base strength, on ion pairing of pyridinium and the carboxylate anion can be seen by comparing the frequencies of the ring breathing mode of pyridinium within the ion-pair complexes. The strongest acid, TFAA, and hence weakest conjugate base, TFA^-, produces pyridinium ion-pair complexes where the ring breathing frequency is the highest. The relative blue shift as compared with the ring breathing mode of pyridine at 990 cm^{-1} is approximately 19 cm^{-1} and dependent upon mole faction as discussed above. Pyridinium/acetate ion pairs, on the other hand, exhibit the smallest relative shift of approximately 14 cm^{-1} (Table 2 summarizes the results).

These frequency-shift data are consistent with the simple molecular orbital/electrostatic model discussed above. A weaker conjugate base will coordinate less well with the pyridinium ion. Consequently, the electronic environment about the hydrogen on the pyridinyl nitrogen will be more like freely solvated pyridinium than for a stronger conjugate base. From the point of view of the simple model, this results in improved delocalization of the π electrons and a higher ring breathing frequency. For the stronger conjugate base, the attraction of the pyridinyl nitrogen to the carboxylate anion will increase. This makes the electronic environment about the pyridinyl nitrogen more like the case of simple hydrogen bonding. Because of this, the delocalization of the π electrons is not as complete as for the weaker anion and the resulting shift in ring breathing frequency is reduced.

TABLE 2: Wavenumber Shifts of the Ring Breathing Mode for Pyridinium Cation/Carboxylate Anion Complexes Relative to the Ring Breathing Mode of Pyridine (989.85 cm^{-1})[a]

carboxylic acid	shift/cm^{-1}	carboxylic acid	shift/cm^{-1}
acetic acid	13.85	propionic acid	14.05
trifluoroacetic acid	18.75,[b] 20.35[c]	*n*-butyric acid	13.95
difluoroacetic acid	17.34[b]	*n*-octanoic acid	13.55
trichloroacetic acid	18.25[c]	pivalic acid	13.85

[a] The estimated error on the shift measurements approximately ±0.50 cm^{-1}. [b] The shift is given for $X_{py} = 0.3$. TFAA and DFAA shows a relatively strong mole fraction dependence for this peak (see Figure 3). [c] The shift is given for $X_{py} = 0.2$.

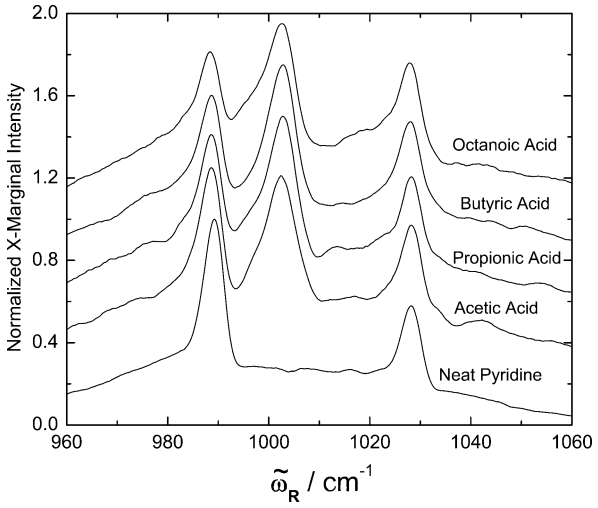

Figure 4. Normalized x-marginal spectra for mixtures of pyridine with the group 2 acids studied in this work ($X_{py} = 0.6$ for all acids shown). See text for a discussion of the qualitative features of these spectra.

To study the impact of steric bulkiness on the structure and dynamics of the pyridine/carboxylic acid solutions, the group 2 acids were used. Figure 4 shows x-marginal spectra from $X_{py} = 0.6$ mixtures of pyridine with acids of varying straight-chain lengths (acetic acid, propionic acid, butyric acid, and octanoic acid) and with pivalic acid. $X_{py} = 0.6$ was chosen because the amount of pyridine and pyridinium are roughly equal. Nearly all the pyridinium is in an ion pair as evident in Figure 4 by the peak position at ~1004 cm^{-1} rather than ~1019 cm^{-1}. It is clear from these data that the bulkiness of the alkane end of the carboxylic acid has very little effect on the strength of the ion pairing with pyridinium. This is not surprising given the similarity in pK_a values (Table 1).

It is interesting to note that the ratio of pyridine to pyridinium decreases with increasing steric bulkiness. Under initial consideration, this result may seem counterintuitive. First, from a pK_a argument, one would expect the opposite trend because acetic acid is a stronger acid than the bulkier acids. However, the pK_a values do not differ by a large amount and, of course, apply quantitatively only to aqueous solutions. Second, one might expect steric crowding to limit the access of pyridine to the carboxylic acid hence resulting in the opposite trend. Third

(and related to the second argument), in polar environments longer-chain acids tend to form stronger dimers[40−44] and hence might be less likely to interact with the pyridine.

The fact that the trend is such that bulkier acids slightly favor pyridinium−carboxylate ion pairs relative to less bulky acids is difficult to understand. Our conjecture is based on a difference in the change in entropy for the mixing/reaction process. First of all, the frequency shift of the ring breathing mode for the ion-paired pyridinium relative to that of pyridine is nearly independent of steric bulkiness of the acid. This suggests comparable enthalpy changes (ΔH) for ion-pair formation. Second, the results indicate the free energy change (ΔG) becomes more negative with steric bulkiness. Taking ΔH to be constant then implies ΔS is less negative for the bulkier cases (ΔS is negative for the pyridine/acetic acid binary mixture[21]). So, it seems a ΔS that is less negative for the bulkier acids may underlie of the observed results. This is presumably reasonable given the fact that carboxylic acids are known to form relatively stable dimers.[40−44] These dimers may be cyclic pairs or open extended chains.[40−44] More bulky acids will tend to adopt the cyclic-pair configuration and hence have lower entropy than less bulky acids that will adopt both cyclic-pair and a variety of open-chain configurations. Consequently, ΔS for the neat acid to the mixture will be less negative for the bulkier acids than for the less bulky acids. A plot of the entropies of formation for the straight-chain carboxylic acids as a function of chain length reveals a slope of 7.76 cal/K per additional carbon.[45] A similar plot of the straight-chain alkanes reveals a larger slope of 8.88 cal/K per additional carbon.[45] Using the straight-chain alkanes as a reference, this gives a 1.12 cal/K per additional carbon entropy deficit for the carboxylic acids. This supports the suggestion that the observed results are a consequence of lower neat entropy of the carboxylic acids.

IV. Conclusions

This work investigates pyridine/carboxylic acid mixtures. The acid−base reaction that occurs in these mixtures produces pyridinium cation and carboxylate anion in a highly product favored reaction. As a result high mole fraction values for pyridinium can be achieved. The pyridinium can be coordinated to a carboxylate anion or freely solvated. The degree of coordination strongly influences the position of the ring breathing frequency of pyridinium, with stronger pairing interaction resulting in a smaller blue shift relative to the ring breathing frequency of neutral pyridine. This behavior can be understood qualitatively using a very simple molecular orbital/electrostatic picture for the electronic behavior of pyridine and pyridinium.

To make the qualitative theory of wider and more practical use, a connection to a more quantitative description must be made. There seems to be at least three distinct avenues to pursue in this regard, each of which will be important in its own right. The first would be to connect with results from computational calculations. The second would be to connect with quantitative analytic theories of hydrogen bonding. The third would be to develop a new theoretical description based on the qualitative picture presented here.

Acknowledgment. We thank Donald Krogstad and Drew Rutherford for valuable discussion and Alex Berg for substaintial improvement in the production of x-marginal spectra. This work was supported by NSF CAREER grant CHE−0341087, the Dreyfus Foundation, and the Concordia College Chemistry Research Endowment.

References and Notes

(1) Welton, T. *Chem. Rev.* **1999**, *99*, 2071.
(2) Ereale, M. J.; Seddon, K. R. *Pure Appl. Chem.* **2000**, *72*, 1391.
(3) Perrin, C. L.; Nielson, J. B. *Annu. Rev. Phys. Chem.* **1997**, *48*, 511.
(4) Vishweshwar, P.; Nangia, A.; Lynch, V. M. *J. Org. Chem.* **2002**, *67*, 556.
(5) Krygowski, T. M.; Szatylowicz, H.; Zachara, J. E. *J. Org. Chem.* **2005**, *70*, 8859.
(6) Kline, C. H., Jr.; Turkevich, J. *J. Chem. Phys.* **1944**, *12*, 300.
(7) Corrsin, L.; Fax, B. J.; Lord, R. C. *J. Chem. Phys.* **1953**, *21*, 1170.
(8) Dugan, M. A.; Mellinger, J. S.; Albrecht, A. C. *Chem. Phys. Lett.* **1988**, *147*, 411.
(9) Dugan, M. A.; Albrecht, A. C. *Phys. Rev. A* **1991**, *43*, 3877.
(10) Dugan, M. A.; Albrecht, A. C. *Phys. Rev. A* **1991**, *43*, 3922.
(11) Schaertel, S. A.; Albrecht, A. C.; Lau, A.; Kummrow, A. *Appl. Phys. B* **1994**, *59*, 377.
(12) Schaertel, S. A.; Lee, D.; Albrecht, A. C. *J. Raman Spectrosc.* **1995**, *59*, 889.
(13) Kozich, V. P.; Lau, A.; Pfeiffer, M.; Kummrow, A. *J. Raman Spectrosc.* **1999**, *30*, 473.
(14) Lau, A.; Kummrow, A.; Pfeiffer, M.; Woggon, S. *J. Raman Spectrosc.* **1994**, *25*, 607.
(15) Stimson, M. J.; Ulness, D. J.; Albrecht, A. C. *Chem. Phys. Lett.* **1996**, *263*, 185.
(16) Ulness, D. J.; Kirkwood, J. C.; Stimson, M. J.; Albrecht, A. C. *J. Chem. Phys.* **1997**, *107*, 7127.
(17) Ulness, D. J.; Stimson, M. J.; Albrecht, A. C. *Chem. Phys.* **1997**, *222*, 17.
(18) Ulness, D. J. *J. Phys. Chem. A* **2003**, *107*, 8111.
(19) Aung, P. P.; Cosert, K. M.; Weisel, L. R.; Schulz, T. F.; Gealy, M. W.; Ulness, D. J. *J. Raman Spectrosc.* **2005**, *36*, 409.
(20) Weisel, L. R.; Ta, T.; Booth, E. C.; Ulness, D. J. *J. Raman Spectrosc.* **2007**, *38*, 11.
(21) Berg, E. R.; Freeman, S. A.; Green, D. D.; Ulness, D. J. *J. Phys. Chem. A* **2006**, *110*, 13434.
(22) Barrow, G. M. *J. Am. Chem. Soc.* **1956**, *78*, 5802.
(23) Golubev, N. S.; Smirnov, S. N.; Gindin, V. A.; Denisov, G. S.; Benedict, H.; Limbach, H.-H. *J. Am. Chem. Soc.* **1994**, *116* 12055.
(24) Akiyama, Y.; Wakisaka, A.; Mizukami, F.; Sakaguchi, K. *J. Chem. Soc., Perkin Trans.* **1998**, *2*, 95.
(25) Limbach, H.-H.; Pietrzak, M.; Sharif, S.; Tolstoy, P. M.; Shenderovich, I. G.; Smirnov, S. N.; Golubev, N. S.; Denisov, G. S. *Chem. Eur. J.* **2004**, *10*, 5195.
(26) Mierzecki, R. *Acta Phys. Polon* **1960**, *19*, 41 (in French).
(27) Singurel, L.; Bazhulin, P. A. *Vestn. Mosk. Gos. Univ. Ser. Fiz. Aston.* **1967**, *1*, 11 (in Russian).
(28) Rezaev, N. I.; Tabibi, M. B. *Russ. Phys. J.* **1976**, *19*, 1159.
(29) Dega-Szafran, D.; Gdanie, M.; Grundwald-Wyspianska, M.; Kosturkiewicz, Z.; Koput, J.; Krzyzanowski, P.; Szafran, M. *J. Mol. Struct.* **1992**, *270*, 99.
(30) Arnett, E. M.; Chawla, B. *J. Am. Chem. Soc.* **1978**, *100*, 217.
(31) Jasinski, J. M.; Brauman, J. I. *J. Am. Chem. Soc.* **1980**, *102*, 2906.
(32) Press, W. H.; Flannery, B. P.; Teukolsky, S. A.; Vetterling, W. T. *Numerical Recipes in C: The Art of Scientific Computing*, 2nd ed.; Cambridge University Press: New York, 1992.
(33) Wolfram, S. *Mathematica 3.0 Standard Add-on Packages*; Cambridge University Press: New York, 1996.
(34) Cotton, F. A.; Poll, R. *Organometallics* **1987**, *6*, 1743.
(35) Muñoz-Caro, C.; Niño, A.; Dávalos, J. Z.; Quintanilla, E.; Abboud, J. L. *J. Phys. Chem. A* **2003**, *107*, 6160.
(36) Zoidis, E.; Yarwood, J.; Danten, Y.; Besnard, M. *Mol. Phys.* **1995**, *85*, 373.
(37) Zoidis, E.; Yarwood, J.; Danten, Y.; Besnard, M. *Mol. Phys.* **1995**, *85*, 385.
(38) Schlücker, S.; Singh, R. K.; Asthana, B. P.; Popp, J.; Kiefer, W. *J. Phys. Chem A* **2001**, *105*, 9983.
(39) Schlücker, S.; Heid, M.; Singh, R. K.; Asthana, B. P.; Popp, J.; Kiefer, W. *Z. Phys. Chem.* **2002**, *216*, 267.
(40) Ng, J. B.; Shurvell, H. F. *J. Phys. Chem.* **1987**, *91*, 496.
(41) Tanaka, N.; Kitano, H.; Ise, N. *J. Phys. Chem.* **1990**, *94*, 6290.
(42) Katchalsky, A.; Eisenberg, H.; Lifson, S. *J. Am. Chem. Soc.* **1951**, *73*, 5889.
(43) Yamamoto, K.; Nishi, N. *J. Am. Chem. Soc.* **1990**, *112*, 549.
(44) Mochizuki, S.; Usui, Y.; Wakisaka, A. *J. Chem. Soc., Faraday Trans.* **1998**, *94*, 547.
(45) NIST Chemistry WebBook, webbook.nist.gov.